Crucial role of oxygen on the bulk and surface electronic properties of stable β phase of tungsten

Ananya Chattaraj, Sebastien Joulie, Virginie Serin, Alain Claverie, Vijay Kumar, Aloke Kanjilal

Crucial role of oxygen on the bulk and surface electronic properties of stable β phase of tungsten

Ananya Chattaraj[1], Sebastien Joulie[2], Virginie Serin[2], Alain Claverie[2], Vijay Kumar[3,4]* and Aloke Kanjilal[1]*

[1]*Department of Physics, School of Natural Sciences, Shiv Nadar University, NH-91, Tehsil Dadri, Gautam Buddha Nagar, Uttar Pradesh 201 314, India*

[2]*CEMES-CNRS and Université de Toulouse, 29 rue J. Marvig, 31055 Toulouse, France*

[3]*Center for Informatics, School of Natural Sciences, Shiv Nadar University, NH91, Tehsil Dadri, Gautam Buddha Nagar, Uttar Pradesh 201 314, India*

[4]*Dr. Vijay Kumar Foundation, 1969 Sector 4, Gurgaon, Haryana 122001, India*

*Corresponding authors: Vijay.kumar@snu.edu.in, aloke.kanjilal@snu.edu.in

Abstract

The A15 β phase of tungsten has recently attracted great interest for spintronic applications due to the finding of giant spin-Hall effect. As β phase is stabilized by oxygen, we have calculated for the first time its electronic structure and found that 20 at.% O-doping makes β phase lower in energy than α-W. Energy dispersive X-ray spectroscopy measurements also show an average of ~16.84 at.% O in 60 nm thick W films which predominantly have β phase as confirmed by grazing incidence X-ray diffraction (XRD). This is in excellent agreement with the simulated XRD of bulk β having 15.79 at.% O. Oxygen binds strongly on the surface and affects the Dirac fermion behavior in pure β-W significantly. There is structural disorder, O-inhomogeneity, and higher density-of-states in O-doped β-W at E_F compared with pure α. These results are promising to understand its higher electrical resistivity and increase in superconducting transition temperature.

The growing interest in spintronic devices has led to much attention on β-W due to the finding of the largest spin-Hall angle (SHA)[1] of around -0.5 among the metallic elements as well as a large spin-orbit torque (SOT).[1,2,3,4] Also, the temperature coefficient of resistivity is nearly zero that is attractive for such applications. Bulk tungsten usually exists in the body-centered cubic (bcc) structure, known as α phase, but a metastable β phase with A15 structure has been found in thin films.[5,6,7,8,9,10] Pure β-W is a topological closed packed structure and interestingly shows multiple Dirac nodal lines and massive Dirac fermion behavior near the Fermi energy (E_F).[11] Experiments show that β-W becomes stabilized in the presence of oxygen.[7,8,10,12,13,14] But an understanding of the electronic structure of O doped β-W is lacking. Here we present for the first-time results of the electronic structure calculations of bulk as well as (001) surface of β-W with O, showing that the bands and Dirac fermion behavior of pure β-W are very significantly affected by O doping. Our calculations show that the introduction of 20 at.% O makes β phase favorable over α and it supports the energy-dispersive X-ray spectroscopy (EDX) and grazing incidence X-ray diffraction (GIXRD) results, while the higher density of states (DOS) at E_F in O doped β-W could possibly be the signature of higher superconductivity transition temperature than that of α.

Earlier, we elucidated the transition of α-W to β phase with 25-30 at.% doping of O by density functional theory (DFT) based *ab initio* molecular dynamics (MD) simulations.[15] However, our GIXRD and EDX experiments showed the formation of the β phase in 60 nm thick W films with 13-19 at.% O, while higher concentrations (16-22 at.%) in 35 nm film led to the formation of a very disordered structure with nanocrystallites of about 2 nm in size.[15] Therefore, a lower oxygen concentration seems to be enough for β-W formation. Also, Demasius *et al.*[1] oxidized 2 nm to 10 nm thick W films by controlled exposure of O and showed that the films were in α phase without O, while ~12.1 at.% O was present in the β films that had the highest SHA. They observed an enhancement in SOT by incorporating O in W films. It was suggested that this

increase was governed by the interface between β-W and FeCoB magnetic film. In a different study using Pt as a heavy metal instead of W, Qiu *et al.*[16] have shown a change in SHA due to the oxidation of the magnetic film by the migrated O from the MgO/SiO_x layers. Accordingly, oxygen in β-W can affect the properties of the thin magnetic film grown on it and the interface.[2,3] Also, interestingly, a higher superconducting critical transition temperature T_c (1 to 4 K) has been reported for β-W compared with 0.01 K in α-W.[17,18,19] The higher T_c is promising for developing detectors for astronomical and quantum information applications.[19,20] According to the Bardeen-Cooper-Schrieffer (BCS) theory, the DOS at the E_F is an important factor and can affect T_c.[21] These applications of β-W and its higher resistivity[2,7,9,22] of 100-300 μΩ-cm compared with ~5.33 μΩ-cm for α-W at room temperature need a proper understanding of the crucial role of O in its stability as well as atomic and electronic structure. The electron-phonon scattering and surface effects were found not to be sufficient to understand the high resistivity. Also, Derunova *et al.*[23] have shown a giant spin-Hall effect in a group of A15 materials and emphasized the location of E_F in the DOS to be very important. However, as we shall show, even a partial oxidation of W affects the electronic structure significantly, making the study of the valence band structure of the β phase important in the presence of O.

The GIXRD patterns of 35 nm (A) and 60 nm (B) thick W films in the 2θ range of 20º to 80º are exhibited in Fig. 1 along with the calculated powder diffraction of 15.79 at.% O doped 2×2×2 supercell of β-W simulated at a high temperature of 3500 K in order to overcome barriers for O diffusion. Here θ is the Bragg angle. The peak centred around 40º for film B belongs to the reflection from either (210) β-W or (110) α-W or both the phases (JCPDS #03-065-6453 for β-W, #04-0806 for α-W). Other two characteristic reflections from the (200) and (211) planes of the β phase along with small peaks around 70º are also identified in film B. The same diffraction pattern was obtained after a long time of more than a year suggesting the stability of the β-W phase. The diffraction pattern of the simulated β-W resembles the one

obtained experimentally for film B. The optimized O doped β-W supercell (inset, Fig. 1) shows a slight deviation from a cube with a small increase in the lattice parameters to 10.32 Å, 10.36 Å, and 10.41 Å compared with the calculated value of 5.059 Å for the unit cell of pure β-W. There is some disorder in the structure along with clustering of O atoms due to the attractive interaction. This leads to inhomegeneity with some regions where no O atom is present. There is a small shift of the calculated diffraction peaks to lower 2θ values compared with the experimental ones due to the slight overestimation of the calculated lattice parameters of pure α (3.171 Å) and β phases compared with the experimental values (3.16 Å and 5.04 Å. These results suggest that an average O concentration of ~15 at.% is good to achieve a stabilized polycrystalline β-W film as also suggested by our EDX experiments discussed below. Importantly, with this O concentration, all the W atoms in a sample may not be in the β phase due to O clustering. Our results therefore suggest the possibility of co-existence of α phase with low O concentration together with β-W with much higher O concentration. Coexistence of α and β phases was also reported by Petroff et al. using transmission electron microscopy (TEM). We also calculated the energies of the 2×2×2 supercell of β-W and 4×4×4 supercell of α-W with the same O concentration and found that the doping of 20 at.% O makes the optimized β-W phase lower in energy compared with α-W after simulated annealing with *ab initio* MD. Therefore, a transition to β phase must occur by this oxygen concentration supporting our experimental results.

Film A (35 nm thick) shows a broad peak centred at around $2\theta = 40^{o}$ from GIXRD (inset, Fig. 1) suggesting it to be disordered. Our *ab initio* MD simulations on higher O concentrations (20 at.%, ~27 at.% and ~30 at.%) in β-W also show an increase in disorder with the broadening of the peaks as demonstrated in Fig. S1 in Supplementary Information. The corresponding increased lattice parameters and energy gain due to O doping are listed in Table S1 in

Supplementary Information. There is a shift of the diffraction peaks to smaller 2θ values and higher gain in energy with increasing O doping.

We further performed EDX measurements in cross-sectional TEM (XTEM) mode parallel to the film surface to understand the distribution of the constituent elements. Figure 2 shows the superimposition of the EDX maps of W, O, Si and Pt (top panel), and the corresponding elemental scans parallel to the surface in three regions near the middle of the film B. It is seen that the average oxygen concentration is (a) 16.76 at.%, (b) 16.93 at.%, and 16.84 at.% with the standard deviation of 9.38 at.%, 9.79 at.%, and 10.31 at.%, respectively. This agrees with our earlier results (Ref. 15) of 13-19 at.% O from scans across the film. However, a close inspection of the EDX map indicates accumulation of O at the W surface. This could happen due to the reaction of the surface W atoms with oxygen because of exposure to ambient atmosphere for more than a month prior to preparing the XTEM sample. The 172 × 46 pixels in the EDX hypermaps with a spot size of 2 nm show that the variation of O concentration is almost similar in the bulk region (traces a-c). However, oxygen is comparatively higher (mean value 41.48 at.%) near the W surface (see Fig. S2 in Supplementary Information). The EDX results of film A for 69 × 28 pixels are shown in Fig. S3 in the Supplementary Information, where the mean O concentration (17.75 at.% with a standard deviation of 5.27 at.% suggesting higher fraction of β) is higher compared with film B.

The calculated DOS of β-W with 15.79 at.% O shows (Fig. 3) a broad peak at ~2.65 eV with a shoulder at ~1.5 eV below E_F. There is a weak peak at ~5 eV. The angular momentum as well as site decomposed partial DOS (PDOS) show that the states appearing in the range of 0 to 6 eV arise dominantly from the W 5*d* orbitals [Fig. 3(a)] and are also present in pure α-W in which case there are two peaks at ~2 eV and ~3 eV. The states beyond this energy arise from the hybridization of O 2*p* with W 5*d* orbitals. Figure 3(b) further indicates an increase in DOS at E_F with increasing O concentration. Interestingly, the DOS at E_F is larger for O doped

β-W compared with pure α case [see Fig. 3(c)]. This is very relevant for the understanding of higher T_c in β-W films. The DOS for β-W with ~15.79 at.% O in Fig. 3(a) and also for a simulated bulk α-W with ~12.3 at.% O in Fig. 3(d) interestingly show broadly similar features, although the starting atomic structures were apparently different. The inset of Fig. 3(d) shows that even in the optimized α phase with lower O concentration, there is a clustering of oxygen due to attractive interaction. Both the O doped phases show a bonding peak due to oxygen at ~7 eV below E_F. The inclusion of spin-orbit coupling (SOC) does not change the DOS significantly except for a small decrease at E_F.

We further studied adsorption of O on (001) surfaces and the DOS for slabs of α-W and β-W are shown in Fig. 4 for clean and with O coverage. The atomic structure (see inset) for 9O (16O) adsorption on α (β) slab shows a small displacement of surface W atoms. In the DOS one can see a broad peak in the W 5*d* band region. Also, the DOS of both α and β slabs show peaks at around -7 eV in Figs. 4(a) and (b). It can be attributed to O bonding interaction as also revealed in doped bulk β-W [Fig. 3(a)] and α-W [Fig. 3(d)]. From these results, the peak at ~7 eV below E_F can be considered to have the joint contribution of W 5*d* and O 2*p* states from bulk and surface of α and β phases. The adsorption energy of an O atom, defined as the gain in energy when a free O atom adsorbs on the surface, for a 4-fold site of α-W and a 3-fold site of β-W on a (001) surface is 7.50 eV and 7.95 eV, respectively. When we considered 9(16) O atoms on (001) surface of α-W (β-W), the adsorption energy becomes 6.76 eV (6.74 eV) per O. This shows a decrease in the adsorption energy of O with increasing coverage, but still these values are much higher than the energy gain of 4.031 eV (3.77 eV) per O for 12.3 at.% (15.79 at.%) O in bulk α-W (β-W) supercell. Therefore, O would be there on the surface of both α and β phases, as evidenced from our experiments (see Fig. 2). Further calculations for an O atom in the sub-surface region give only a small (0.223 eV) decrease for α-W but a significantly

lower value for β-W. Accordingly, O is likely to be present in sub-surface sites also for α-W, but go to the bulk region in β-W.

Our calculations for bulk β-W also give a peak (Fig. 3) in the region of 8.6-9.4 eV below E_F, while for the bulk α-phase the peak extends to slightly higher binding energies. These peaks are also identified to arise from the hybridization of O and W valence orbitals. However, when O is adsorbed on the surface, the DOS has low value in this region and these results are not affected much by including SOC. Accordingly, we conclude that there are two peaks at around -7 eV and -9 eV associated with oxygen bonding states in both bulk α and β phases. These results may vary to some extent depending upon the presence of defects and/or interfaces such as between α and β phases in actual samples which are not considered in our calculations.

In order to further understand the effects of O doping on the band structure near E_F, we performed calculations on a unit cell of β-W with the doping of one and two O atoms. These correspond to 11 at.% and 20 at.% O doping, respectively, covering the range of O concentration of interest. The fully relaxed atomic structure and the unit cell are shown in inset in Fig. S4. The optimized lattice parameters are 5.122 Å, 5.253 Å, and 5.128 Å (space group Pm) for the case of one O and 5.286 Å, 5.286 Å, and 5.069 Å for 2 O doping (space group P1). The corresponding DOS are also shown in Fig. S4 and these do not have a peak at around 7 eV below E_F. Therefore this peak in O-doped α- and β-W can be associated to arise from clustering of O atoms. The band structures for the pure β (without and with SOC) and O-doped cases are shown in Fig. 5. The band structure for the pure case has multiple Direc points and nodal lines near E_F and agree well with the published results.[11] Inclusion of SOC splits the band degeneracy and opens up small band gaps (Fig. 5b) at some places. Doping of O clearly leads to significant changes in the band structure as seen in Figs. 5c and d for the doping of 1 O and 2 O in β-W unit cell, respectively. It has been further found that inclusion of SOC leads to splitting of bands as shown in Fig. S5 in the Supplementary Information. In order to further compare the results,

we have chosen nearly equivalent directions in the BZ (see Fig. S6 in Supplementary Information) and the corresponding bands are shown in Fig. 6. Here, the energy bands for the pure β case in Γ-X-M directions (Fig. 6a) having multiple Dirac points near the E_F, get affected when one O is doped, but the Dirac point-like feature can still be seen along the Y–C direction. The bands in the Γ-Y direction change significantly compared with the Γ-X direction for the pure case. Further, with the doping of 2 O atoms, the bands have changed more significantly. Inclusion of SOC changes the band structure further significantly as shown in Fig. S7.

We further explored the nature of O bonding by performing Bader charge analysis which shows an excess charge (~1.6e) at O predominantly due to transfer from the nearest neighbour W atoms. A large fraction of W atoms has charge in the range of 5.5-6.0e and only a few of them have charge in the range of 5.0-5.5e, suggesting that the charge transfer from W to O is much smaller than in WO_3. The hybridization of partially filled 5*d* orbitals of W with the O 2*p* orbitals gives rise to an increase in DOS near E_F and below ~-6 eV (Fig. 3), while a decrease in the remaining *d*-band region of W. The charge density and electron localization function (ELF) isosurfaces are shown in Fig. S8 which are localized around O ions. It is also realized that the doping of O brings disorder in the structure and consequently there is broadening of peaks in the DOS. The disorder in the structure as well as inhomegenous distribution of O is expected to lead to higher resistivity of such samples as observed while an increase in DOS at E_F can contribute to an increase in T_c.

In summary, we have shown for the first time using *ab initio* MD that the β-W phase becomes favorable over α with the doping of ~20 at.% O. Also our calculations show that oxygen is distributed inhomegenously due to clustering and there could be coexistence of α and β phases. These results are in agreement with EDX analysis showing a mean of 16.84 at.% O in bulk with fluctuation in O concentration. The evolution of stable β phase by doping O in W films was manifested by GIXRD and has been supported by our calculations, which also show O

induced disorder in the structure. The electronic structures of O doped bulk β-W as well as α-W show bonding peaks of O 2*p* orbitals with 5*d* of W at ~7 and ~9 eV below E_F but the peaks in the *d* band region are distinct. There is a characteristic broad peak at around 2.6 eV in the W 5*d* band region of β-W in contrast to peaks at ~2 and 3 eV in pure α-W. There is an increase in DOS at E_F in the O-doped β phase with respect to pure α-W. This study would therefore be a benchmark for opening the window to understand the higher T_c in β-W. Oxygen is found to interact strongly on W surfaces and therefore it supports the observed increase in O concentration in the surface region. These results would be interesting for further studies of the surfaces and interfaces of β-W films and their frontier applications, while O induced disorder could be a factor for higher resistivity. We believe that this combined experimental and theoretical study will help in further understanding of the technologically interesting β phase of W.

Acknowledgements

AC and AK acknowledge the financial support from Shiv Nadar University and also from the Department of Science and Technology, India under the project No. DST/EMR/2014/000971. The help received from Dr. D. Kabiraj and Mr. Abhilash of Inter University Accelerator Centre, New Delhi for electron beam deposition of W films is highly acknowledged.

Author contributions

A.Ch. found the problem, designed the work, grew thin films by electron beam deposition and studied the structure by XRD. V.S., A.C. and S.J. did the EDX measurements. A.K. and A.Ch did the experimental analysis. V.K. and A.K. planned the theoretical work. V.K. and A.Ch. did the calculations and performed analysis. V.K., A.K., and A.Ch. wrote the manuscript.

Competing interests

The authors declare that they do not have any competing financial interest.

METHODS

Sample preparation and measurements

A 500 μm thick Si(100) wafer was diced into pieces (area 1×1 cm^2) and cleaned by dipping in trichloroethylene, acetone, isopropanol, and deionized water followed by heating for 2 min in each step. After cleaning of the Si surface, W films of about 35 nm (A) and 60 nm (B) thickness were grown at room temperature (RT) by electron beam deposition technique. The deposition rate was 0.01 nm/s, while the chamber base pressure and the working pressures were ~6.65 $\times 10^{-7}$ mbar and 1.33×10^{-6} mbar, respectively. We used 99.95% pure W powder (Alfa Aesar) for depositing films whose thickness was estimated by a surface profilometer (DektakXT, Bruker). The β-W phase was confirmed by GIXRD measurements (Bruker, D8-Discover) using the Cu-K_α radiation (λ = 0.154 nm). The elemental analysis has been performed by EDX with a 2 nm spot size in the cross-sectional geometry of TEM. The mapping has been taken parallel to the film surface. We used a C_s corrected TEM system from Tecnai-FEI operated with an acceleration voltage of 200 kV. A Pt layer was deposited on the W film to avoid any damage during the XTEM sample preparation by focused ion beam. The full range of the EDX hypermap has 172 (69) values in a column for each element in every raster scan for sample B (A).

Calculations on bulk and surfaces

The calculations have been performed within the framework of DFT as implemented in the Vienna Ab initio Simulation Package (VASP).[24] We used Perdew-Burke-Ernzerhof (PBE)

form of the generalized gradient approximation (GGA)[25] for the exchange-correlation functional and projected augmented wave (PAW) pseudopotentials[26] for electron-ion interaction. The kinetic energy cut-off for the plane wave expansion of the wave function was set to 500 eV. The atomic structures in all cases were completely relaxed until the absolute value of each component of the Hellmann-Feynman force on each ion became less than 0.005 eV/Å. We also performed the volume relaxation. A grid of 15×15×15 (9×9×9) Monkhorst-Pack **k**-points was used for the unit cell calculations of the α (β) phase, whereas 5×5×5 **k**-points were used for the 4×4×4 (2×2×2) supercell calculations for structural relaxation and the convergence of the charge density. The lattice parameters of the optimized unit cells of 1) α-W (bcc, Im-3m) with 2 atoms per unit cell and 2) β-W (A15, Pm-3n) containing 8 atoms per unit cell, are found to be 3.171 Å and 5.056 Å, respectively. These are in good agreement with the previously reported values of 3.17 Å and 5.05 Å as well as our experimental results.[1,2,4,15] For the 2×2×2 supercell of β-W phase (64 atoms) the optimized lattice parameter was found to be 10.110 Å. Oxygen with 15.79 at.% concentration was initially distributed in β-W supercell keeping the O-O separation of about 2.04 Å as obtained for the case of two O atoms. This oxygen concentration lies in the range of 13-19% obtained from the EDX measurement[15] on sample B. Subsequently we performed *ab initio* MD simulations to explore energetically the most favorable configuration using the simulated annealing method. For this, the system was heated to 3500 K and equilibrated for 3 ps. Then the system was cooled from 3500 to room temperature continuously by simulating for 3.5 ps. In these finite temperature calculations, we used only the Γ point to represent the Brillouin zone. After cooling to room temperature, we optimized the structure by relaxing the ions as well as the cell parameters using again 5×5×5 **k**-points mesh with high precision. Similar calculations were performed for other oxygen concentrations as well as for α-W. The (001) surface of β-W was modelled by a slab of 3 unit-cell thickness (108 W atoms) with about 15 Å vacuum space. We considered 2×2 (3×3)

supercell in the plane of the slab for β-W (α-W with 99 atoms) and a 5×5×1 **k**-points mesh to perform Brillouin zone integrations. The ions were relaxed keeping the cell dimensions fixed. Further we studied adsorption of O atoms at 4-fold (3-fold) site on the (001) surface of α and β as well as on a sub-surface site in order to compare the behavior with bulk. Bader charge analysis has been conducted to check the valence electrons on W and O atoms.

Figures

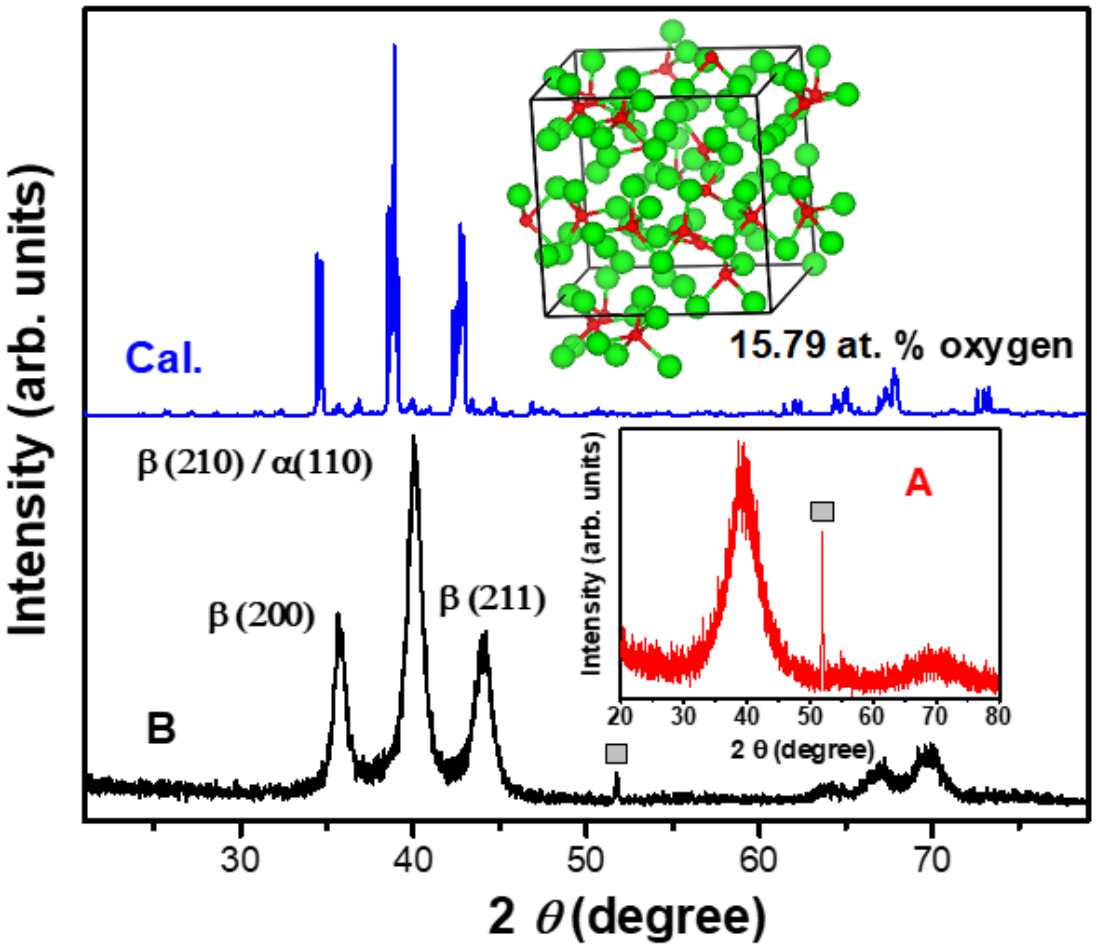

Figure 1 X-ray diffraction and atomic structure. X-ray diffraction pattern of film B (60 nm thick) with characteristic peaks of the β phase and possible presence of α phase due to the overlapping (110) peak. The calculated powder X-ray diffraction of 15.79 at. % O doped β-W obtained from *ab-initio* MD simulations reproduces the features quite well. The corresponding atomic structure is shown in the inset. The green and red balls are W and O atoms, respectively. The measured diffraction pattern of film A (35 nm thick) is shown in the inset. There is a broad peak signifying the presence of disorder in the structure. The peak marked with a grey box is the reflection from the Si substrate.

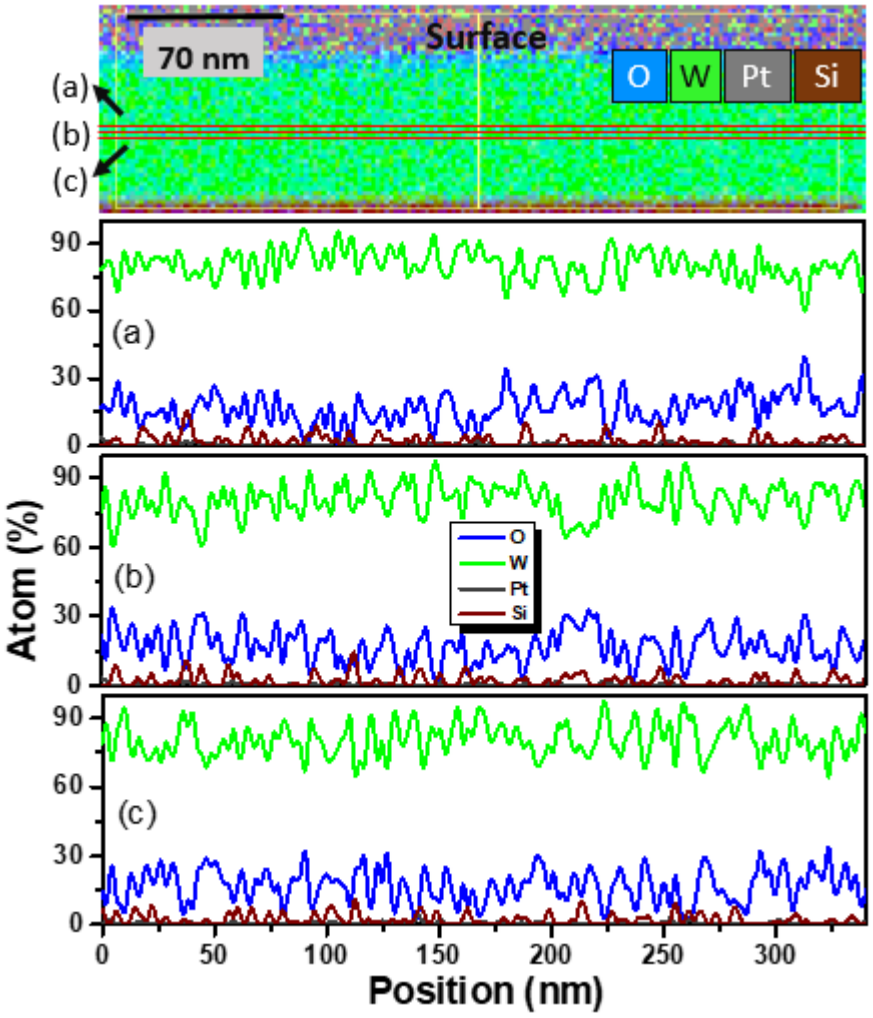

Figure 2 Elemental distribution in 60 nm thick film by EDX. The superimposed elemental EDX maps show the distribution of W (green), Si (brown), O (blue) and Pt (gray) in cross-sectional mode. It reveals the existence of O throughout the W film, but there is an increase in O concentration at the surface (see Fig. S2). The elemental profiles along the traces, marked by 3 red lines (a), (b) and (c) in the middle of the W film (top panel), are projected in the below panels showing the average oxygen concentration of (a) ~16.76 at.%, (b) 16.93 at.%, and (c) 16.84 at.% with the standard deviation of 9.38 at.%, 9.79 at.%, and 10.31 at.%, respectively, showing a significant variation on the averall trend. The Si and Pt signals within the W film are below the noise level.

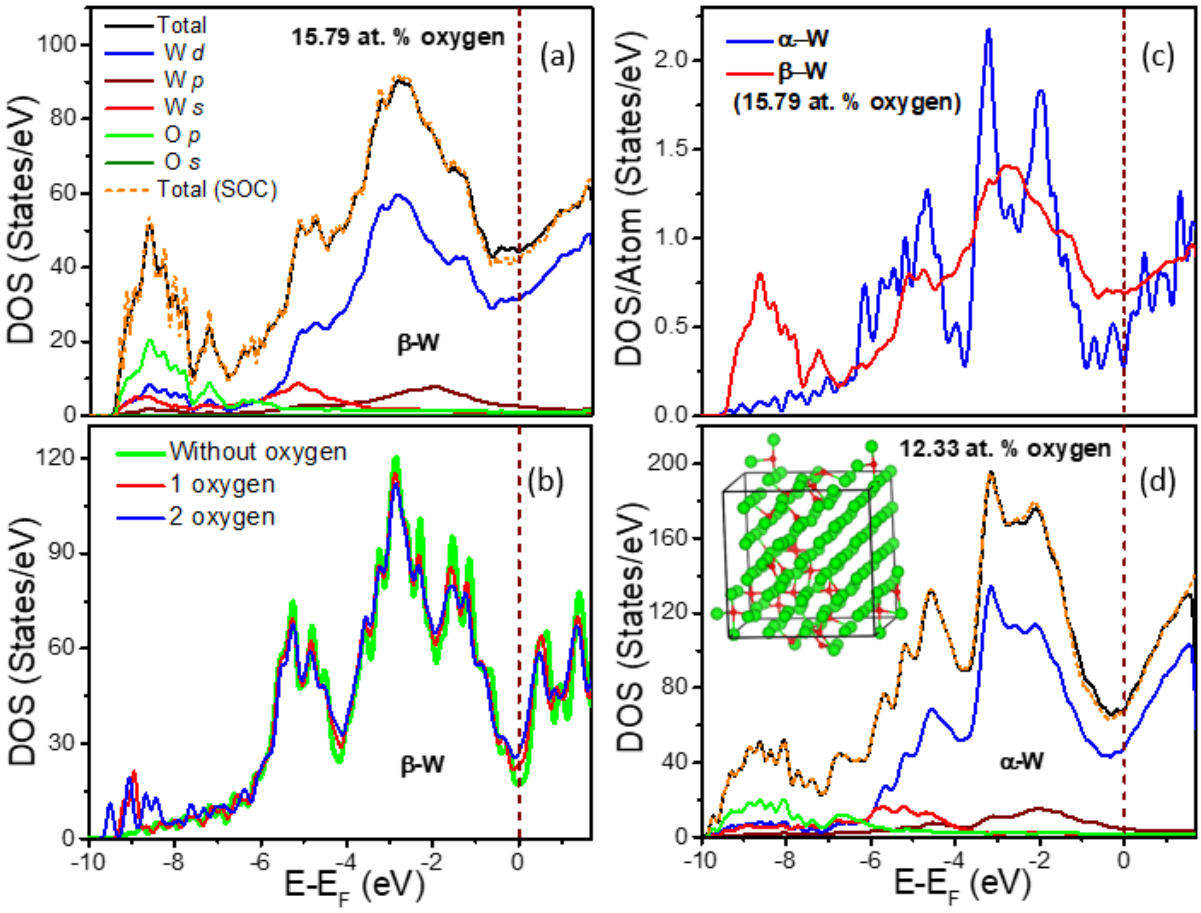

Figure 3 Electronic structure of bulk α- and β-W with O doping and spin-orbit coupling. (a) The total density of states (TDOS) with and without spin-orbit coupling (SOC) for a 2×2×2 supercell of β-W doped with 15.79 at.% O. Site and angular momentum projected density of states (PDOS) are shown without SOC. (b) The calculated DOS of a pure 2×2×2 supercell of β-W, and with one and two oxygen doped in it, shows an increase in the DOS at the Fermi level with the number of dopant. (c) The DOS per W atom for 15.79 at.% O doped β-W shows a significant enhancement at E_F compared with the value for pure α-W. (d) The TDOS with and without spin-orbit coupling for 4×4×4 supercell of α-W doped with 12.33 at.% O. The site and angular momentum projected DOS are also shown. The optimized atomic structure of α-W (green balls) showing clustering of oxygen (red balls) is given in the inset. The wine color dashed line shows the Fermi level at 0 eV in all the cases.

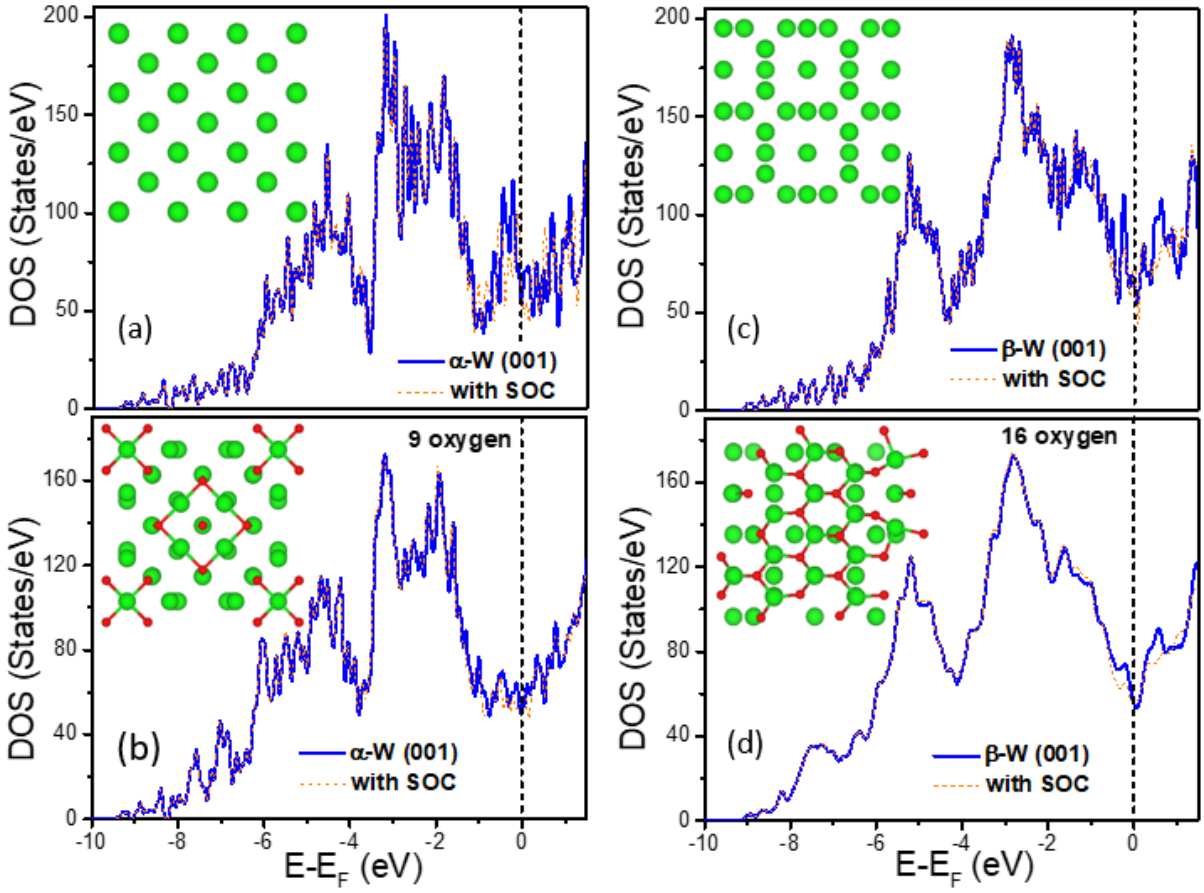

Figure 4 Atomic and electronic structure of slabs of α- and β-W without and with O adsorption. (a) and (c) TDOS for a slab of α-W and β-W, respectively, with (001) surface (inset shows the side view of the slab in the cell) without and with SOC. (b) and (d) TDOS of (001) slab of α-W with 9 oxygen on 4-fold sites and β-W with 16 oxygen atoms on 3-fold sites in the cell, respectively, without and with SOC. The inset shows the top view of the slab in the cell. Some relaxation of W atoms can be seen particularly for α-W slab. Green (red) balls show W (O) atoms and the vertical broken line shows the Fermi energy E_F.

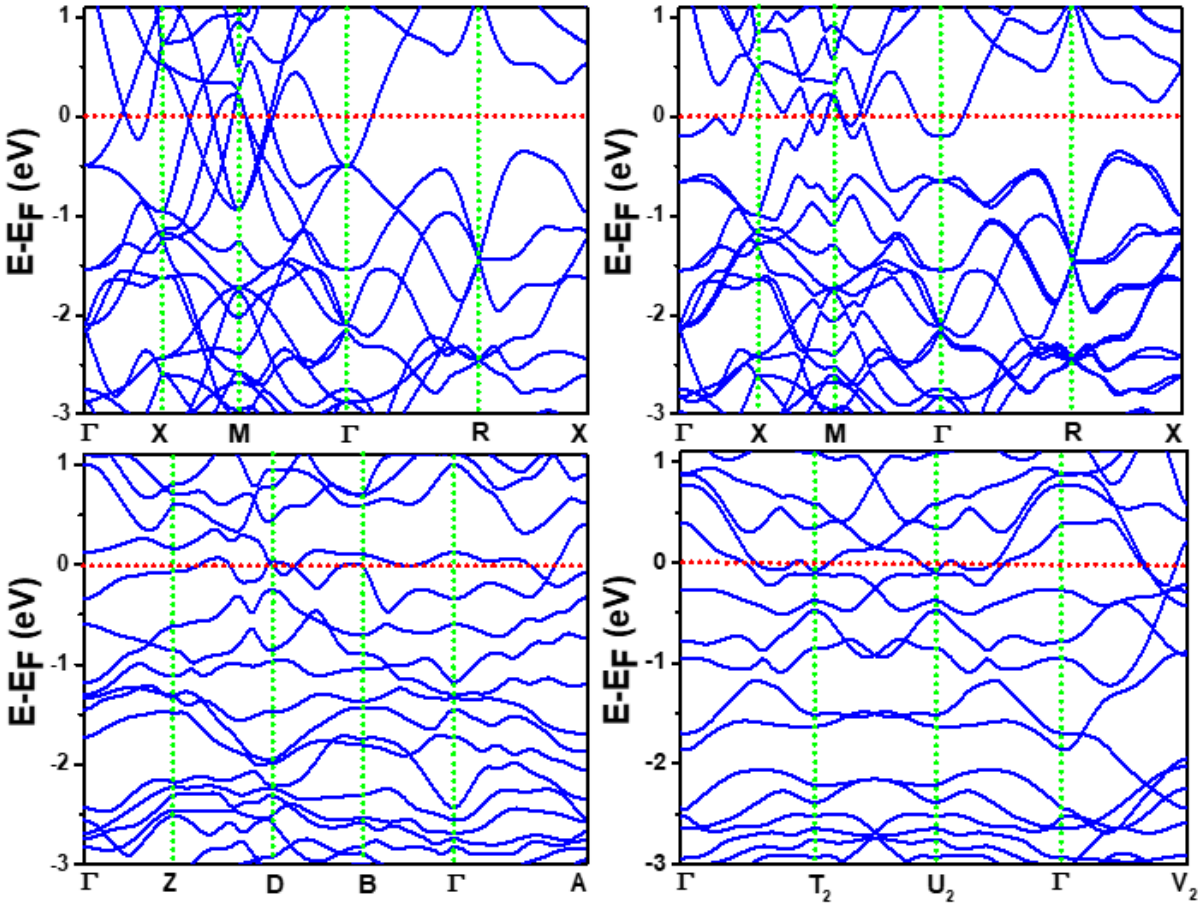

Figure 5 Band structure of pure and O doped β-W. (Upper panels) Band structure of pure β-W without (left) and with SOC (right). SOC has significant effect on the energy bands near the Fermi energy which has been taken to be the zero of energy. (lower panel) Band structure for one O (left) and two O (right) in a unit cell of β-W without SOC. The doping of O creates distortion in the unit cell leading to reduced symmetries with Pm and P1 space groups, respectively.

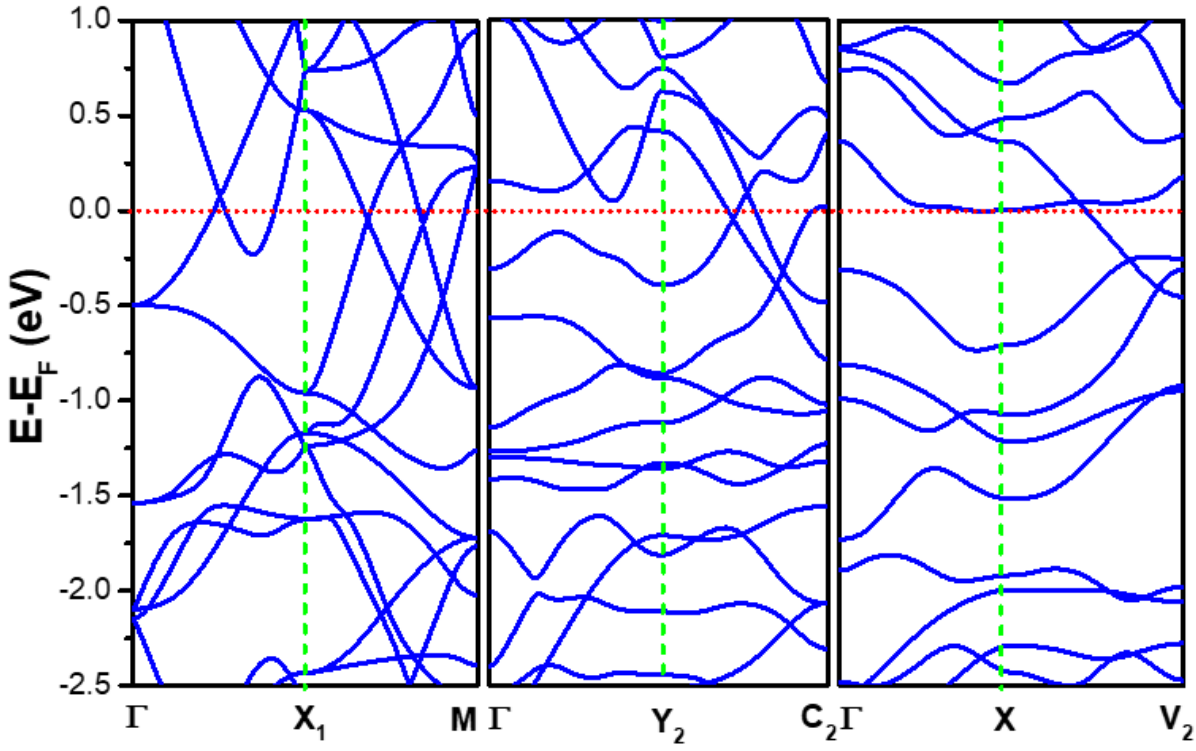

Figure 6. Effects of oxygen doping on energy bands of β-W. (a) – (c) show the energy bands for the unit cells of undoped, one O doped, and two O doped β-W, respectively, considering nearly equivalent directions in the respective Brillouin zones.

References

1. Demasius, K. U., Phung, T., Zhang, W., Hughes, B. P., Yang, S. H., Kellock, A., Han, W., Pushp, A. and Parkin, S. S. Enhanced spin–orbit torques by oxygen incorporation in tungsten films. *Nat. Comm.* **7,** 1-7 (2016).
2. Pai, C. F., Liu, L., Li, Y., Tseng, H. W., Ralph, D. C. and Buhrman, R. A. Spin transfer torque devices utilizing the giant spin Hall effect of tungsten. *Appl. Phys. Lett.* **101,** 122404 (2012).
3. Hao, Q. and Xiao, G. Giant spin Hall effect and switching induced by spin-transfer torque in a $W/Co_{40}Fe_{40}B_{20}/MgO$ structure with perpendicular magnetic anisotropy. *Phys. Rev. Appl.* **3,** 034009 (2015).
4. Sui, X., Wang, C., Kim, J., Wang, J., Rhim, S. H., Duan, W. and Kioussis, N. Giant enhancement of the intrinsic spin Hall conductivity in β-tungsten via substitutional doping. *Phys. Rev. B* **96,** 241105(2017).
5. Davey, W. P. The lattice parameter and density of pure tungsten. *Phys. Rev.* **26,** 736 (1925).
6. Charlton, M. G. & Davis, G. L. Allotropes of tungsten. *Nature* **175,** 131-132 (1955).
7. Petroff, P., Sheng, T. T., Sinha, A. K., Rozgonyi, G. A. and Alexander, F. B. Microstructure, growth, resistivity, and stresses in thin tungsten films deposited by rf sputtering. *J. Appl. Phys.* **44,** 2545-2554 (1973).
8. O'keefe, M. J. & Grant, J. T. Phase transformation of sputter deposited tungsten thin films with A-15 structure. *J.Appl. Phys.* **79,** 9134-9141 (1996).
9. Rossnagel, S. M., Noyan, I. C. and Cabral Jr, C. Phase transformation of thin sputter-deposited tungsten films at room temperature. *J. Vac. Sci. Technol. B* **20,** 2047-2051 (2002).
10. Choi, D. Phase transformation in thin tungsten films during sputter deposition. *Microelec. Eng.* **183,** 19-22 (2017).
11. Li, J., Ullah, S., Li, R., Liu, M., Cao, H., Li, D., Li, Y. and Chen, X.Q. Topological massive Dirac fermions in β-tungsten. *Phys. Rev. B* **99,** 165110 (2019).
12. Shen, Y. G., Mai, Y. W., Zhang, Q. C., McKenzie, D. R., McFall, W. D. and McBride, W. E. Residual stress, microstructure, and structure of tungsten thin films deposited by magnetron sputtering. *J. Appl. Phys.* **87,** 177-187 (2000).
13. Shen, Y. G. & Mai, Y. W. Influences of oxygen on the formation and stability of A15 β-W thin films. *Mater. Sci. Eng. A* **284,** 176-183 (2000).

14. Narasimham, A. J., Medikonda, M., Matsubayashi, A., Khare, P., Chong, H., Matyi, R. J., Diebold, A. and LaBella, V. P. Fabrication of 5-20 nm thick β-W films. *AIP Adv.* **4,**117139 (2014).

15. Chattaraj, A., Balal, M., Yadav, A. K., Barman, S. R., Sinha, A. K., Jha, S. N., Joulie, S., Serin, V., Claverie, A., Kumar, V. and Kanjilal, A. Unravelling oxygen driven α to β phase transformation in tungsten. *Sci. Rep.* **10,** 14718 (2020).

16. Qiu, X., Narayanapillai, K., Wu, Y., Deorani, P., Yang, D. H., Noh, W. S., Park, J. H., Lee, K. J., Lee, H. W. and Yang, H. Spin–orbit-torque engineering via oxygen manipulation. *Nat. Nanotech.* **10,** 333-338 (2015).

17. Chopra, K. L. Enhancement of superconductivity in tungsten films. *Phys. Lett. A* **25,** 451-452 (1967).

18. Basavaiah, S. and Pollack, S. R. Superconductivity in β-Tungsten Films. *J. Appl. Phys.* **39,** 5548-5556 (1968).

19. Lita, A. E., Rosenberg, D., Nam, S., Miller, A. J., Balzar, D., Kaatz, L. M. and Schwall, R. E. Tuning of tungsten thin film superconducting transition temperature for fabrication of photon number resolving detectors. *IEEE Trans. Appl. Supercond.* **15,** 3528-3531 (2005).

20. Young, B. A., Saab, T., Cabrera, B., Cross, J. J. and Abusaidi, R. A. Tc tuning of tungsten transition edge sensors using iron implantation. *Nucl. Instr. Meth. Phys. Res. A* **444,** 296-299 (2000).

21. Mata-Pinzón, Z., Valladares, A. A., Valladares, R. M. and Valladares, A. Superconductivity in bismuth. A new look at an old problem. *PLoS One* **11,** 0147645 (2016).

22. Hao, Q., Chen, W. and Xiao, G. Beta (β) tungsten thin films: Structure, electron transport, and giant spin Hall effect. *Appl. Phys. Lett.* **106,** 182403 (2015).

23. Derunova, E., Sun, Y., Felser, C., Parkin, S. S. P., Yan, B. and Ali, M.N. Giant intrinsic spin Hall effect in W_3Ta and other A15 superconductors. *Sci. Adv.* **5,** 8575 (2019).

24. Kresse, G. and Joubert, D. From ultrasoft pseudopotentials to the projector augmented-wave method. *Phys. Rev. B* **59**, 1758–1775 (1999).

25. Perdew, J. P., Burke, K. and Ernzerhof, M. Generalized gradient approximation made simple. *Phys. Rev. Lett.* **77,** 3865 (1996).

26. Blöchl, P. E. Projector augmented-wave method. *Phys. Rev. B* **50,** 17953 (1994).